Electric Power Systems Research 190 (2021) 106846

Contents lists available at ScienceDirect

Electric Power Systems Research

journal homepage: www.elsevier.com/locate/epsr

High impedance fault detection based on linear prediction

Reginaldo B.G. Grimaldi[a], Talita S.A. Chagas[a], Jugurta Montalvão[b], Núbia S.D. Brito[c], Wellinsílvio C. dos Santos[d], Tarso V. Ferreira[b,*]

[a] Postgraduate Program in Electrical Engineering (PROEE), Federal University of Sergipe (UFS), São Cristóvão 49.100-000, Brazil
[b] Department of Electrical Engineering, PROEE, UFS, São Cristóvão 49.100-000, Brazil
[c] Department of Electrical Engineering (DEE), Federal University of Campina Grande (UFCG), Campina Grande 58.109-970, Brazil
[d] Technology Center of the Federal University of Alagoas (UFAL), Alagoas, 57.072-970, Brazil

ARTICLE INFO

Keywords:
Alternative transients program
Capacitor bank switching
High impedance faults
Linear predictor
Load energization

ABSTRACT

In many situations, conductor rupture in distribution systems or even its contact with structures external to the systems (such as trees) does not sensitize protection systems. This type of occurrence and its variations are typically called high impedance faults. The present work proposes a method for detection of high impedance faults based on linear prediction. Concerning validation of the method, a database was created through simulations performed in the Alternative Transients Program, based on a real energy distribution system. In addition to high impedance faults, load energization and capacitor bank switching situations were also simulated in order to test the robustness of the method against probable false positives. From obtained results, a decision criterion was developed aiming at the detection of high impedance faults based on the linear predictor of current signals through time, which obtained success rates above 80 % for real data.

1. Introduction

Electric Power Distribution Systems (EPDS) are exposed to various disturbances and anomalies that affect the operation of electric networks. Among numerous perturbations, High Impedance Faults (HIF) are some of the major concerns, and can occur when an energized cable, either ruptured or unruptured, contacts with a high impedance surface, such as a tree branch. In the occurrence of a HIF, the fault current shows low amplitude, having the same order of magnitude as other typical phenomena of an EPDS, such as load energization (LE) or a capacitor bank switching (CBS). According to [1], usual protection devices activated by overcurrent cannot detect such faults.

Concerning HIF episodes occurrence, in addition to compromising the quality of the service, power distribution companies may suffer sanctions stipulated by regulatory agencies, which evaluate and regulate - in several aspects - the electric power supply.

According to [2], the service continuity is of paramount importance, since it affects people's daily life and causes major disruptions by compromising essential services to the consumer. The ideal situation is no interruption in electricity supply. In case of any interruption, it should be minimal, and informed to the consumer in a timely manner, in order to prevent possible losses arising from lack of energy [2]. However, in case of HIF, the interruption of power supply may be much longer than the typical one, since the time between occurrence of the cut in the supply and perception of the non-attendance of the consumers by the power company may depend on the fault detection.

Nevertheless, financial losses and intangible damages associated with the image of power companies are not the most concerning consequences of HIF. Accidents, health risks for animals and people, eventually leading to death, are in fact, the most tragic consequences.

Several studies based on techniques for detection and location of HIF have been developed in recent years. In the 1980's, many works were published proposing the analysis of signals from HIF in the time domain [3]. In relation to the frequency domain, some studies have highlighted the use of low frequency harmonic components [4]. In 1988, Huang et al [5] evaluated the performance of four different algorithms for HIF detection by means of a stage failure test using proportional relays, second and third harmonic current relays, and ground fault relays. Already in 1990, Emanuel et al [6] carried out extensive measurements of harmonic currents in HIF in sandy terrain to evaluate the extent in which the harmonic currents can be used for HIF detection.

More recently, many research findings have been published involving voltage unbalance [7, 8], traveling wave theory [9, 10], discrete wavelet transform (DWT) [11–14] and analysis of harmonic content [15–19].

* Corresponding author.
E-mail address: tarso@ufs.br (T.V. Ferreira).

https://doi.org/10.1016/j.epsr.2020.106846
Received 25 May 2020; Received in revised form 12 August 2020; Accepted 9 September 2020

The voltage unbalance method is based on voltage monitoring after conductor disruption. Vieira and others [7] presented a method for detecting and locating HIF using an approach based on voltage unbalance. The results showed that the algorithm effectively identifies broken conductors, either with or without ground contact faults, located on the load or source side. Malagod [8] also proposes a HIF protection system based on voltage unbalance along the feeder. Through simulations, the author demonstrated that the voltage unbalance allows detecting the conductor disruption, with the installation of sensors connected to the network. In the event of a fault, only the downstream sensors would act. Voltage unbalance based techniques, however, may not be reliable in cases where there is no conductor breakage, as in faults caused by conductor contact with trees.

Methods based on traveling waves rely on the analysis of the high frequency signal components. Lopes and others [9] described a fault location algorithm that performs transient detection by applying Park transformation. Silva [10] presented a technique based on the reflection and refraction of the electric impulses of voltage or current at the fault point. However, traveling waves based methods have high demands of both, sampling rates and computational processing, which significantly increases implementation costs.

Other HIF detection techniques are based on Discrete Wavelet Transform (DWT). Hafidz and others [11] proposed a method, which analyses the wavelet coefficients of the current signals through an artificial neural network, and obtained success rates of 67%. Santos and others [12] technique aimed to detect HIF and other transient phenomena associated with distribution system disturbances employing DWT. Results have shown good average performance, but also room for improvement. Despite of the DWT advantages, designing a systematic detection technique based on this transform is challenging, due to subjectivity in mother wavelet choice and loss of resolution through decomposition.

A harmonic content analysis technique was presented by Gomes and others [15], aiming to detect HIF in the grass and reducing the risk of fire. Results were encouraging, however its applicability was demonstrated only for faults in vegetated soil, excluding HIF occurrence in other soils. Yeh and others [16] proposed the use of sliding fast Fourier and Walsh-Hadamard transform to extract the entire low-frequency spectrum, both amplitude and phase. According to their results, the method could detect the fault in two cycles, however, the capacity of distinguishing HIF from other disturbances was not presented.

Although significant research has been carried out for the detection of HIF in distribution systems, there is a strong need for the development of new methods that can efficiently and reliably detect HIF, since none of the techniques presented so far has been consolidated in practice.

In this context, this work presents a method capable of detecting HIF based on the current signal analysis, using the linear prediction, which presents lower computational cost and has no dependence on network topology. The parameter for HIF detection comes from error between current signal and its linear prediction. The proposed method performance was evaluated with real data and Alternative Transients Program (ATP) simulated data. Tests with signals from capacitor bank switching and load energization, which produce characteristics similar to those of HIF were also performed, in order to evaluate the robustness of the method against false positives. Finally, the proposed technique is compared to a wavelet based method.

This paper is organized as follows: Section 2 describes high impedance faults; Section 3 presents linear predictor, the method used for detecting HIF; Section 4 describes the methodology used in the development of the work. Section 5 presents the results with the detection method based on the linear predictor. And finally, section 6 presents conclusions along with future work.

2. High impedance fault

The main characteristic of a HIF is the low amplitude of the currents, which is mainly caused by the rupture of the energized conductor and its contact with a high impedance surface such as sand, asphalt, gravel, grass and pavement [2]. During the phenomenon, before the cable comes into contact with the ground, an electric arc may occur, since when the energized cable approaches the ground, potential difference increases and the electric field becomes more intense, reducing the resistance of the air, which facilitates the air conduction process [20]. The occurrence of the electric arc in the HIF gives rise to some characteristics in the waveforms of the current signals of a HIF, which are:

- Intermittence: process related to the formation and extinction of the electric arc during the HIF [20];
- Asymmetry: magnitude of the positive half-cycle greater than that of the negative half-cycle. This characteristic is attributed to porosity and moisture of the contact surface [6];
- Non-linearity: resultant of different resistivities from the several layers of the soil [18];
- Buildup: fault current envelope growth. During this phenomenon, the amplitude can remain constant before growing back, giving rise to the phenomenon called shoulder [20].

All these features are illustrated in Fig. 1.

With respect to the frequency domain, the characteristics of the current signals of the HIF produce a harmonic behavior, which may be used to detect the HIF. According to Nakagomi [20], the HIF currents produce the following spectral components:

- The distortion in the waveform, due to the non-linearity of the arc resistance leads to the appearance of low order harmonics in the current (third to tenth harmonics, approximately);
- The asymmetry between the half-cycles is responsible for the presence of even-order harmonics;
- The intermittence of the current during the formation and the extinction of the arc leads to the appearance of a high frequency harmonics spectrum;

The buildup and shoulder phenomena cause variation of the current amplitude over time, producing inter-harmonics resulting from the dynamic behavior of the defect contact resistance.

3. Linear predictor

The linear predictor (LP) is a mathematical method aimed at

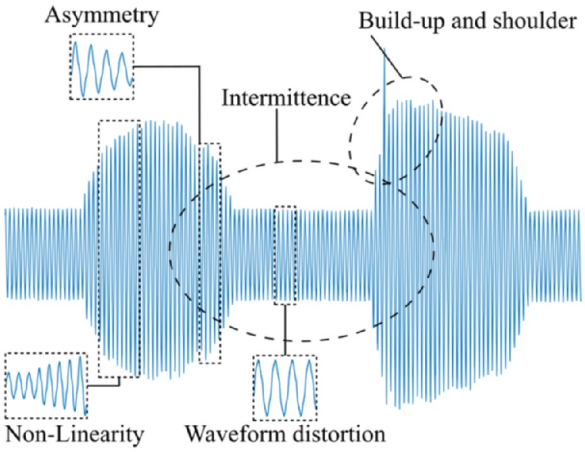

Fig. 1. HIF characteristics.

predicting the value of a sample in a sequence as a linear combination of the former ones. The weighting coefficients are obtained by comparison between observed and predicted values [21]. LP is considered a powerful technique for predicting time series in a time-varying environment. The linear prediction model recursively represents time series of signal samples over a time interval [22], such as:

$$y(t+T) = C_1 \cdot y(t) + C_2 \cdot y(t-T) + \ldots + C_m \cdot y(t-(m-1)\cdot T) + e(t+T), \quad (1)$$

wherein C_1, C_2, ..., C_m are the linear prediction coefficients or weighting coefficients, m is the model order, T the sampling time, $y(t+T)$ the future observation and $y(t)$, $y(t-T)$, ..., $y(t-(m-1)T)$ are the present and past observations, and $e(t+T)$ is the model error. In (1), the output is the linear combination of the current and past samples, hence it is called the linear prediction [22].

Eq. (1) is also called an all-pole model, a reference to the Z-domain representation of the corresponding transfer function, where the prediction error, $e(n)$, is taken as input signal, whereas $y(n)$ is regarded as an output signal. As a result, the all-pole model in the frequency domain is given by (2):

$$H(z) = \frac{1}{1 - \sum_{k=1}^{m} C_k \cdot z^{-k}} \quad (2)$$

For the prediction of HIF signals it was necessary to define the model degree, that is, m (which should be carefully selected, as detailed in section V) and the coefficients, C_1, C_2, ..., C_m, which must be calculated from the modeling window. The purpose of the prediction applied to HIF signals is to use waveform modeling to predict future signal samples. The prediction error is the difference between the predicted and actual values, which can play the role of transient indicator.

The block diagram of the linear predictor is presented in Fig. 2, wherein $y(n)$ represents the original signal, $\hat{y}(n)$ the signal predicted and $e(n)$ the prediction error. The predicted value of the signal $y(n)$ is given by (3):

$$\hat{y}(n) = C1 \cdot y(n-1) + C2 \cdot y(n-2) + \ldots + Cm \cdot y(n-m) \quad (3)$$

To determine the coefficients C_1, C_2, ..., C_m, the pseudoinverse was used, as given in (4) and (5):

$$[\hat{Y}] = [Y] \cdot [C] \quad (4)$$

$$C = (Y^T \cdot Y)^{-1} \cdot Y^T \cdot \hat{Y}. , \quad (5)$$

wherein $\hat{Y}$ is the predicted signal, Y is the original signal and C is the prediction coefficients vector.

The error generated between the predicted value and the actual value is (6):

$$e(n) = y(n) - \hat{y}(n). \quad (6)$$

Due to dynamic regime deviation, we should expect that, when HIF occurs, a remarkable prediction error variation should occur as well, which may constitute a fault detection trigger.

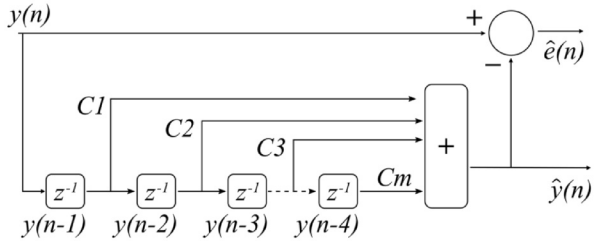

Fig. 2. LP block diagram.

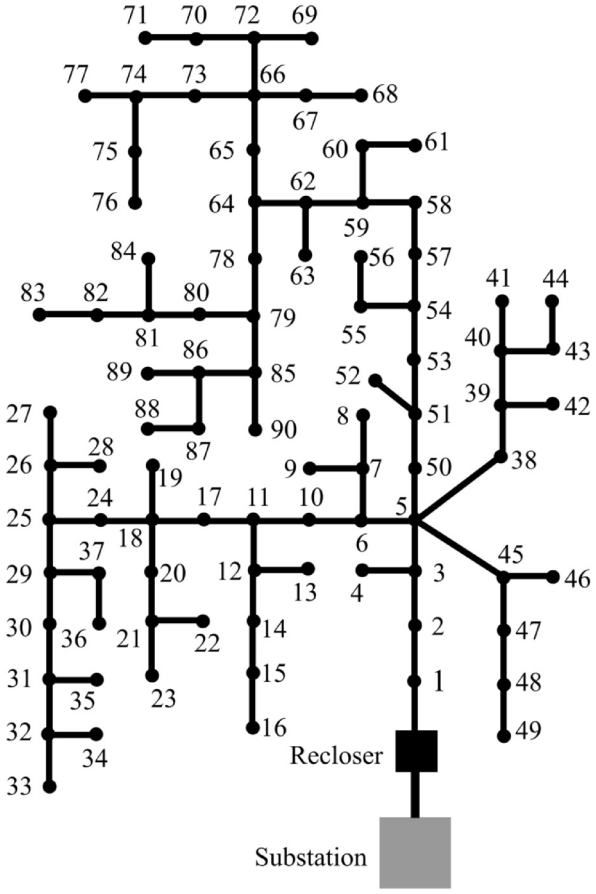

Fig. 3. Distribution feeder (test system), adapted from [2].

4. Methodology

In order to allow the development and test of the proposed detection algorithm, a database containing HIF, CBS and LE signals was built, based on signals obtained through ATP simulations. Besides HIF current signals, load energization (LE) or a capacitor bank switching (CBS) were also simulated.

The HIF simulations were generated from a model proposed in [2], which was able to reproduce the main characteristics of a HIF, that is: nonlinearity, asymmetry, intermittence, buildup and shoulder. To construct the model, [2] used oscillographic records resulting from field experiments, considering six types of soils (dry and wet): sand, asphalt, pavement, gravel and local land. Simulations of HIF based on the model proposed in [2] were applied to a real distribution system from a Brazilian electricity utility, whose diagram is presented in Fig. 3.

The test-system was modelled considering the following characteristics [2]:

- Operating voltage: 13.8 kV.
- Neutral regime: isolated.
- No capacitive compensation.
- Radial topology.
- Non-transposed three-phase lines at distributed and constant parameters.
- Stretches consisting of cable 4 AWG.
- Loads near points along the feeder, grouped on a single bus, resulting in a feeder with 90 buses.
- Skin effect factor of 0.33 for the cables.
- Ground resistivity of 350 Ωm.
- Constant impedance model for the loads, which are considered as parallel resistor-inductor (RL) circuits connected between each

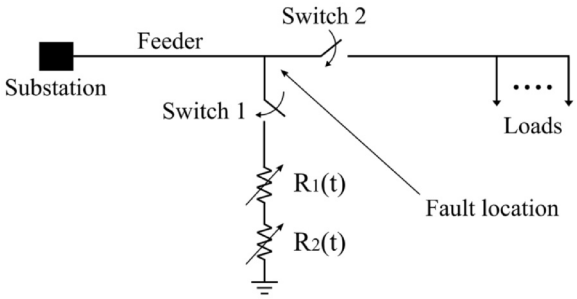

Fig. 4. HIF model [2].

phase of each bus and the ground.
- Average power factor of 0.955.

The HIF model used to emulate the fault's main characteristics is presented in Fig. 4, which is composed by [2]. The model is composed by:

- Two time-varying resistances (TVRs), in series, and controlled by Transient Analysis of Control Systems.
  - Resistance R1: simulates the characteristics of nonlinearity and asymmetry (providing the same characteristics at every cycle of the signal).
  - Resistance R2: simulates the phenomena of buildup and shoulder (just influencing at the beginning of the signal).
- Two time-controlled switches:
  - Switch 1: connects the resistances to the fault point and simulates the fault inception time.
  - Switch 2: connected downstream from the fault point, simulating the conductor breakage.

The LE and CBS events were simulated in the same test system in the following way:

- The load energizations were simulated by connecting significant loads to the system, as in a system recomposition. For example, by energizing all buses, from 54 onwards, by connection with bus 53. Transients are expected to occur for a few cycles after switching, followed by an increase of the currents upstream of the bus connection;
- The switching of capacitor banks was simulated considering a bank of 1.8 Mvar (usual value in distribution systems). Transients are expected to occur at the time of switching for a few cycles.

The used simulation variables were: fault location, contact surface, load conditions, and fault inception angle. Only faults between one phase and ground were simulated because HIFs are considered monophasic [2].

The considered load conditions varied between 25 to 100% by 25% of installed capacity. The fault inception angle varied between 0 to 180° by 30°. Nine among ninety buses were chosen as fault locations, which were buses 10, 23, 30, 44, 49, 56, 63, 68 and 90.

In real applications, the recorded voltage and current signals are subject to the presence of noise. Thus, it was necessary to perform noise modeling on the simulated signals. According to [5], the noise in power systems measurements has a normal probability distribution, and it is present throughout the whole recorded signals, irrespectively if the record is either with or without disturbances. Signal-to-noise ratio (SNR) is presented in (7):

$$SNR_{dB} = 20 \cdot log\left(\frac{A_{sign}}{A_{noise}}\right) \tag{7}$$

The current observed in the substation of the test system (recloser in bus 1) was used as the only input parameter for the proposed classification process. In this way, voltage information is not required. The sampling rate employed was 15360 Hz, which is the typical sampling frequency adopted by digital disturbance recorders (DDR). Finally, the current signals of the simulated phenomena (HIF, LE, CBS) underwent a windowing process with a width of 5 cycles, with a step of one cycle at a time [18]. In this windowing process it was possible to define how many samples should have HIF characteristics to the point of sensitizing the algorithm. This information is very important, as it has a decisive influence on the applicability of the methods in real time HIF detector systems.

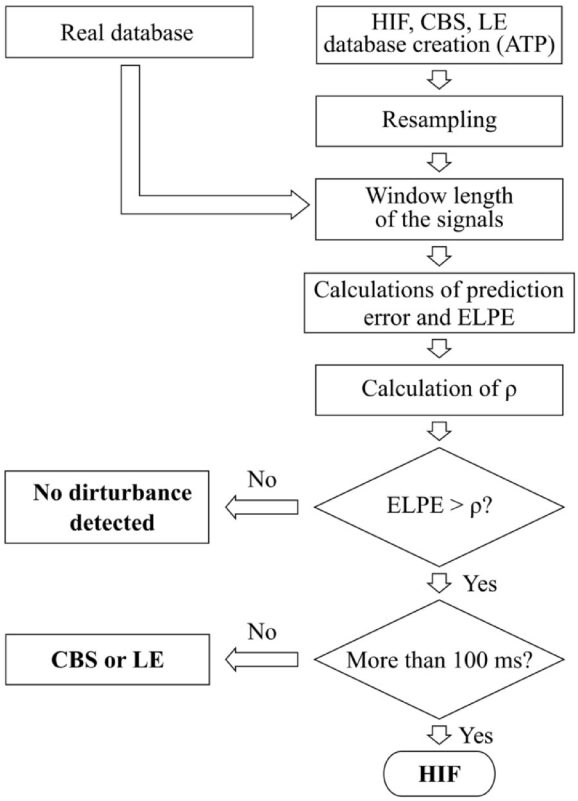

Fig. 5. Proposed methodology.

A second database, composed of real oscillographic records of HIF obtained from field experiments [2], was also used to validate the method. The main characteristics of the whole database are shown in Table 1.

In the development of the algorithm, the LP model was initially defined, including its order, according to the theory presented in Section 3. Methodology flow is illustrated in Fig. 5.

The model output, when compared to a database signal, gives rise to an error signal whose energy is referred as ELPE (error energy of the linear predictor), a basic parameter to detect and classify the phenomena through the proposed method. The use of ELPE also has advantages for minimization of spurious noises that can make the classification task difficult. Energy was calculated from a sliding window of fixed size equal to 128 samples (half cycle). The window moves sample-by-sample sequentially, while at each step the window energy is calculated.

Then, a threshold was used for detection and classification of HIF compared to other disorders. The threshold ρ used is adjusted based on the ELPE values and is calculated at each window [23] (8):

$$\rho = (1 + \eta) \cdot \max(ELPE_{past}) \tag{8}$$

Where $ELPE_{past}$ represents the energy of the prediction error of the past window; *max()* is a function to compute the global maximum value

among analyzed energy samples; and η is a secure margin.

The calculation of the threshold ρ is done repeatedly until the first sample exceeds it. This instant indicates that electromagnetic transients have been detected. Then, the threshold is kept constant and equal to the value calculated in that window before the crossing. This allows spurious variations not affecting the detection of disturbances, and prevents the threshold from being above the energy values when the system is subjected to disturbances. Both HIF, CBS and LE, cause an increase in the ρ threshold, however in the last two phenomena this increase tends to be maintained for a relatively short period of cycles (typically five). Thus, the detection time used was 100 milliseconds, which is equivalent to 6 (six) cycles. Thereby, if the ELPE indicator persists for less than 100 milliseconds, the occurrence of a CBS or a LE can be considered. Otherwise, the detection of a HIF is considered.

It stands out that several scenarios were simulated to define the best predictor order and threshold. Those scenarios included real and simulated waveforms, which were randomly divided into adjustment and validation sets, in the proportion of 30% and 70%, respectively. Each scenario was run 10 times.

5. Results analysis

The method for diagnosis of HIF proposed in this work is based on the analysis of electromagnetic transients induced by HIF to detect disturbances and to differentiate it from other phenomena, thus avoiding false positives.

As placed in the Methodology Section, two parameters must be determined: LP order and threshold. Linear predictors of orders 2, 4, 6, 8 and 10 were tested, combined with a secure margin of 0.1; 0.2; 0.3; 0.4 and 0.5. The success rate of the test sets for all scenarios are shown in Table 2.

Regarding the choice of η, the values of 0.3, 0.4 and 0.5 obtained similar results and, considering the statistical nature of the presented results, it can be inferred that these results are statistically equivalent. However, by objectively evaluating Table 2, it is observed that the predictor of 10th-order with a η of 0.5 obtained the best results.

Considering the LP order, it is noticeable from Table 2 that 2 and 4 had the most unsatisfactory performance, either for simulated or real signals database. The performance of the LP of order 6, 8 and 10, presented a performance similar to each other; however, for the real database, the predictor of order 10 obtained a better performance. A success rate of more than 90% was obtained for predictors of order 6, 8, 10 with η of 0.3, 0.4 and 0.5 for simulated data.

It is also important to note that the 10th-order LP can model up to the 5th harmonic of the analyzed signal, which corroborates findings of other researchers who focus their analysis in the 2nd, 3rd and 5th harmonics to detect HIF [18, 23–25].

The 10th-order LP with a η of 0.5 was applied to the adjustment sets of the database (30%) and the calculation of the ELPE for HIF, CBS and LE signals. Both HIF, CBS and LE cause an increase in ELPE, however, in CBS and LE this increase is not maintained for more than 5 (five) cycles.

In Figs. 6, 7 and 8 the results of the currents observed from the substation are presented (bus 1).

In Fig. 6, the predicted error and ELPE of a HIF in bus 10 of the test system on a gravel surface with load conditions in 75% is shown. Fig. 7 presents the same results of an LE between bus 17 and 18 of the test system with load conditions in 75%. In Fig. 8, a CBS is shown in bus 9 of the test system with load conditions in 75%.

Table 1
Database

Phenomenon		Number of Records
Simulations	HIF	214
	CBS	316
	LE	264
Real	HIF	27
Total		**281**

Table 2
Scenarios rate for test set.

Order	Threshold	Simulations			Real
		HIF	CBS	LE	HIF
2	0.1	97.31%	17.81%	19.07%	44.44%
	0.2	91.50%	54.38%	55.10%	74.07%
	0.3	88.14%	85.69%	84.79%	66.67%
	0.4	83.22%	97.41%	95.57%	59.26%
	0.5	78.07%	99.54%	98.26%	46.15%
4	0.1	52.12%	26.18%	22.54%	48.15%
	0.2	96.86%	73.67%	72.06%	82.37%
	0.3	95.75%	94.82%	92.87%	77.77%
	0.4	93.28%	98.93%	98.07%	74.07%
	0.5	89.04%	100%	99.81%	59.26%
6	0.1	100%	26.18%	24.66%	74.07%
	0.2	100%	74.12%	72.06%	88.58%
	0.3	100%	94.98%	95.28%	83.48%
	0.5	98.65%	99.24%	98.07%	81.57%
8	0.1	100%	27.39%	27.55%	59.26%
	0.2	100%	78.38%	72.45%	88.88%
	0.3	100%	96.19%	94.60%	86.38%
	0.4	99.32%	99.69%	99.42%	85.18%
	0.5	98.21%	100%	99.61%	81.48%
10	0.1	100%	22.83%	16.57%	48.15%
	0.2	100%	77.01%	65.70%	92.59%
	0.3	99.55%	96.04%	90.01%	85.18%
	0.4	98.65%	99.39%	96.15%	82.40%
	0.5	96.64%	100%	98.65%	87.48%

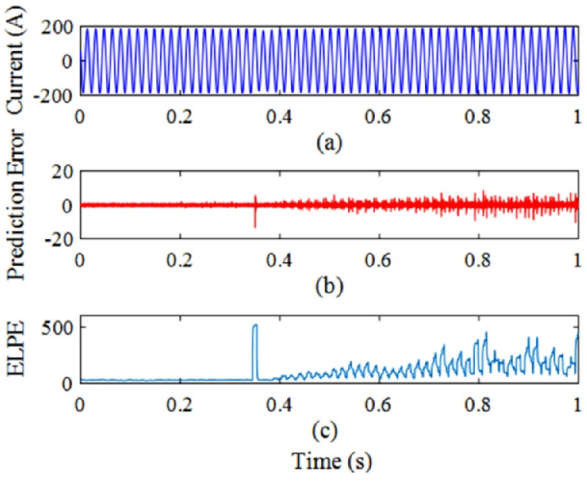

Fig. 6. Result of the processing of a HIF in gravel, in bus 10: (a) Current Ia; (b) Prediction Error; (c) ELPE.

It can be noticed that in HIF there is a change in prediction error and ELPE, and this behavior remains throughout the observation window of the phenomenon, as shown in Fig. 6. In the specific case in the phenomena of LE and CBS (Fig. 7 and 8) there is a change in prediction error and ELPE, however this change lasts only a few milliseconds. Soon after, the error and energy return to normal operation values.

Figs. 9, 10 and 11 show details of HIF detection process based on LP. The parameters used are still 10th-order and $\eta = 0.5$. The evaluation of the threshold crossing is made in each processing window, repeatedly, until the threshold is exceeded by the first sample that indicates a transient. If the energy value exceeds the limit for more than 6 cycles (100 ms), the algorithm will determine that a HIF has been detected.

In Fig. 9 (a) the ELPE is shown for the entire duration of the phenomenon observed. In Figs. 9 (b) to (e), plots of this phenomenon are observed in smaller time windows. Fig. 9 (b) presents the event immediately before the occurrence of HIF (257.7 ms at 341.1 ms). It is

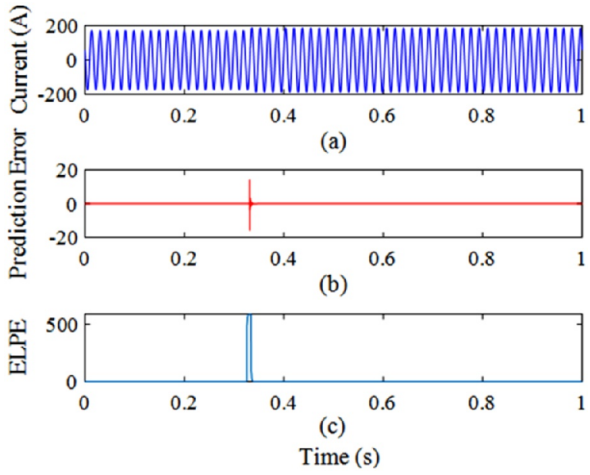

Fig. 7. Result of the processing of a LE between buses 17 and 18: (a) Current Ia; (b) Prediction Error; (c) ELPE.

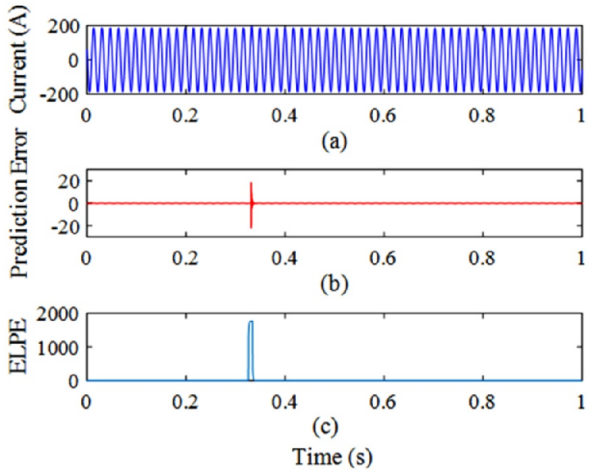

Fig. 8. Result of the processing of a CBS in bar 9: (a) Current Ia; (b) Prediction Error; (c) ELPE.

noticed that the threshold (red dashed line) is not crossed. Fig. 9 (c) presents the ELPE, when the first sample obtained during HIF is considered (257.8 ms at 341.2 ms).

In the first sample, ELPE crosses the threshold (at the extreme right of the graph). It is important to emphasize that, as the ELPE value increases intensely, it turns the samples previously present in the window (before 341.2 ms) imperceptible, resembling a line close to zero. Then, in Fig. 9 (d), the ELPE window allows three cycles to be observed during the fault (307.8 ms at 391.2 ms). This well-featured event corresponds to the buildup and shoulder period. In Fig. 9 (e) the ELPE is shown six cycles after the onset of HIF (357.8 ms at 441.2 ms). The ELPE values persist in exceeding the threshold.

In Fig. 10, an example of the result of applying the algorithm proposed to CBS can be observed. In Fig. 10 (a), as in Fig. 9, ELPE is shown for the entire duration of the phenomenon observed. In Fig. 10 (b) the event is observed before the occurrence of CBS (238.4 ms at 321.8 ms). It is noticed that the threshold is not crossed. Fig. 10 (c) presents the ELPE when the first sample performed during CBS is considered (238.5 ms at 321.9 ms).

In the first sample, ELPE crosses the threshold (at the extreme right of the graph). Afterwards, in Fig. 10 (d), the ELPE is shown during 288.5 ms at 371.9 ms, and the threshold is crossed twice, with final values of the ELPE below the threshold. In Fig. 10 (e) the ELPE is shown six cycles after the onset of CBS (338.5 ms at 421.9 ms). The ELPE values no longer cross the proposed threshold.

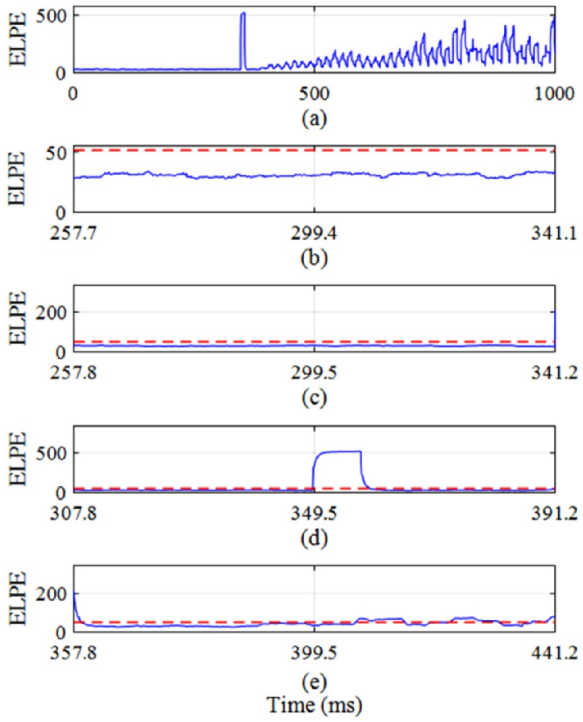

Fig. 9. Energy result of HIF in bus 10 on the sand surface: (a) Complete sign of HIF; (b) One cycle before HIF; (c) 1st sample with HIF; (d) 3 cycles after HIF onset; (e) 6 cycles after HIF onset.

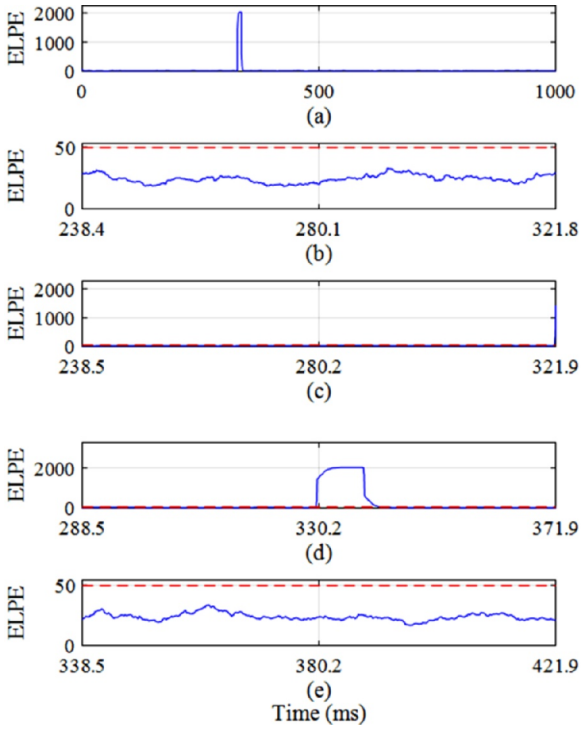

Fig. 10. Energy result of CBS in bus 9: (a) Complete sign of CBS; (b) One cycle before CBS; (c) 1st sample with CBS; (d) 3 cycles after CBS onset; (e) 6 cycles after CBS onset.

In Fig. 11, results of a LE are presented. The similarity with CBS curves, shown in Fig. 10, is noticeable. In both cases it is possible to distinguish the curves in relation to a HIF six cycles after the beginning of the phenomena.

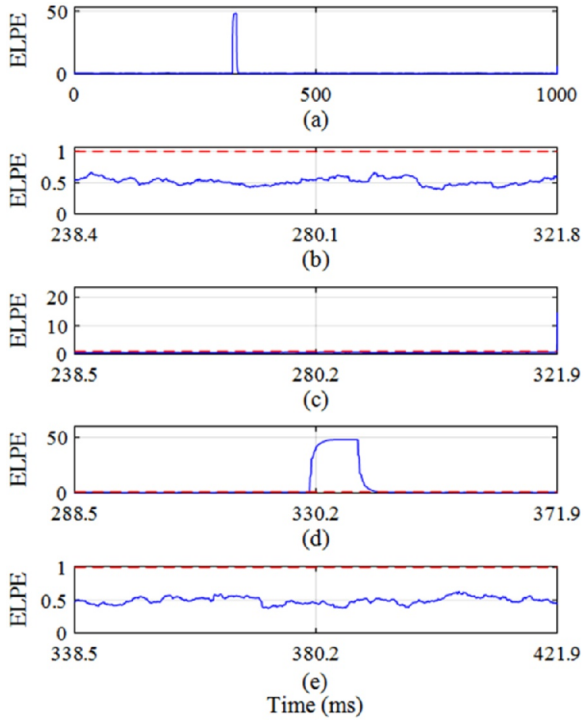

Fig. 11. Energy result of LE between buses 11 and 12: (a) Complete sign of LE; (b) One cycle before LE; (c) 1st sample with LE; (d) 3 cycles after LE onset; (e) 6 cycles after LE onset.

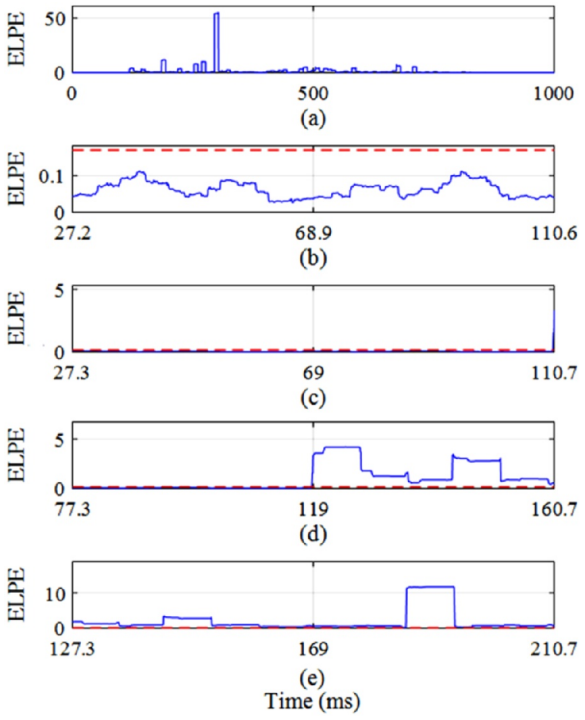

Fig. 13. Result of the processing of a HIF (Real Data) by the LP algorithm: (a) Complete sign of HIF; (b) One cycle before HIF; (c) 1st sample with HIF; (d) 3 cycles after HIF onset; (e) 6 cycles after HIF onset.

5.1. Evaluation of the real data method

After the method had been tested with simulated data, real oscillography records of HIF were used for validation. An oscillography of the current signal of a HIF on a wet gravel surface, as well as the results of the predicted error and ELPE are presented in Fig. 12.

As noticed in Fig. 12, in HIF there is a change in prediction error and ELPE, and this behavior remains throughout the observation window of the phenomenon, as presented in Fig. 6.

The experiment took place in a low load feeder, so the current is low, but even so, the method was able to detect HIF. It should be noted that the current and potential transformers interference did not disable the detection of the electromagnetic transients [2].

It is also observed that the variations in the current signal are considerable, however the overcurrent protection did not act in these cases [2]. With the results, the secure margin η was established in 0.5. The results obtained from the application of the detection algorithm of a HIF on a wet gravel surface are shown in Fig. 13.

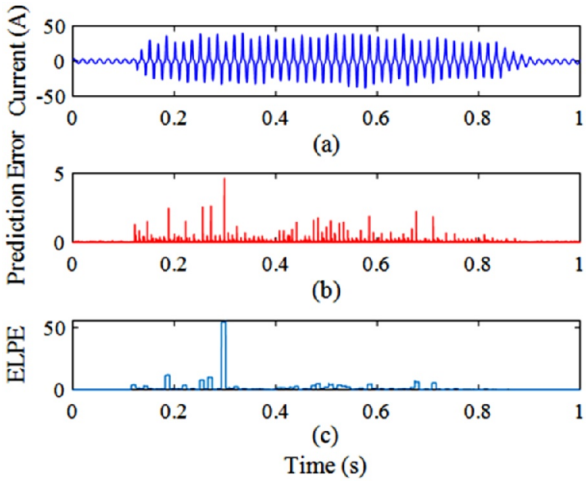

Fig. 12. Result of the processing of a HIF (Real Data) by the algorithm LP: (a) Current Ia; (b) Prediction Error; (c) ELPE.

The results shown in Fig. 13 are organized as in Fig. 8. In Fig. 13 (a) the whole 1 second time window is presented. Fig. 13 (b) presents the event immediately before the occurrence of HIF (27.2 ms at 110.6 ms). It is noticed again that the threshold is not reached. Fig. 13 (c) presents the ELPE when the first sample performed during HIF is considered (27.3 ms at 110.7 ms).

In the first sample, ELPE crosses the threshold (at the extreme right of the graph). In Fig. 13 (d), the ELPE window allows to observe three cycles during the fault (77.3 ms at 160.7 ms), where we can see the variations of ELPE generated by the buildup and shoulder phenomena. In Fig. 13 (e) the ELPE is presented six cycles after the onset of HIF (127.3 ms at 210.7 ms), and it is observed that the ELPE values persist in exceeding the threshold, as expected and obtained during the tests with simulated signals.

At the end, it has been concluded that the HIF detection method proposed in this work has performed satisfactorily in all cases, proving to be effective, even in cases where the amplitude variation of the current is small.

5.2. Comparison with Wavelet based method

Wavelet based techniques for HIF detection has been a vigorous research theme. In this work, the DWT based technique proposed by [12] was implemented for comparative purposes. In [12], the HIF signals were decomposed by DWT (Daubechies 4) wavelet. The energy of first level wavelet coefficients was calculated and used as the detection parameter of HIF, similarly to the role played by the EPLE in this work. The linear predictor used in this case was a 10th-order model with a threshold of 0.5. The same evaluation methodology was used in both methods. Each scenario was run 10 times and the average results are presented in Table 3.

Table 3
Scenarios success rate for test set.

Methods	Simulations			Real
	HIF	CBS	LE	HIF
LP	96.64%	100%	98.65%	87.48%
TWD	85.4%	100%	92.25%	76.67%

It is possible to notice that the linear prediction obtained better results than the DWT based method. Furthermore, as described in [12], the HIF detection time using the DWT-based method is up to 150 ms, while in the method proposed in this paper, the time limit is 100 ms, demonstrating that the LP-based method is also faster.

6. Conclusion

This paper proposes the use of a technique for the HIF detection in electrical systems. The technique in question uses the energy raising of linear predictor error signals as indicator of HIF. It has also demonstrated the robustness of the method against eventual false positives, when other disturbances with similar behavior, such as load energization and capacitor bank switching occur.

The results obtained with linear prediction have demonstrated the method viability, which can correctly distinguish the transient period of occurrence in the first sample where the targeted phenomena occurs (i.e. HIF).

Both threshold and LP order that had the best performance and efficiency for the analyzed database were 50% and 10, respectively, both for real and simulated cases.

Regarding the classification of the disorders, the method was selective, presenting reliable results and maximum rate of success. For both, real and simulated cases, detection and classification are performed in up to 100 milliseconds, lower than the maximum time adopted in Brazil for detection of transient disturbances (150 milliseconds) [18].

However, it is still necessary to evaluate the method in the presence of phenomena such as inrush currents or nonlinear loads. Increasing the prediction order is a promising path, aiming to deal with such phenomena. Additionally, the impact of the distributed generation on the algorithms performance must be evaluated, as well as its applicability in other systems (e.g. the IEEE 14 bus) and neutral regimes. Also, Fourier transform based variations of the method must be implemented, in order to verify the occurrence of beneficial model regularizations.

CRediT authorship contribution statement

Reginaldo B.G. Grimaldi: Conceptualization, Methodology, Software, Validation, Writing - original draft, Visualization. **Talita S.A. Chagas:** Conceptualization, Software, Validation, Writing - original draft. **Jugurta Montalvão:** Conceptualization, Methodology, Writing - review & editing, Formal analysis. **Núbia S.D. Brito:** Validation, Formal analysis, Resources, Writing - review & editing. **Wellinsílvio C. dos Santos:** Validation, Formal analysis, Resources, Writing - review & editing. **Tarso V. Ferreira:** Validation, Resources, Writing - original draft, Writing - review & editing, Visualization, Supervision.

Declaration of Competing Interest

The authors declare that they have no known competing financial interests or personal relationships that could have appeared to influence the work reported in this paper.

Acknowledgements

This study was financed in part by the Coordenação de Aperfeiçoamento de Pessoal de Nível Superior - Brasil (CAPES) - Finance Code 001, and also partially supported by Conselho Nacional de Desenvolvimento Científico e Tecnológico – CNPq.

References

[1] J.C. García, V.V. García, N. Kagan, Detection of high impedance faults in overhead multi grounded networks, 2014 11th IEEE/IAS International Conference on Industry Applications, Juiz de Fora, 2014, pp. 1–6, https://doi.org/10.1109/INDUSCON.2014.7059480.
[2] W.C. dos Santos, B.A. de Souza, N.S.D. Brito, F.B. Costa, M.R.C. Paes, High impedance faults: from field tests to modeling, J. Control Autom. Electr. Syst. 24 (6) (2013) 885–896.
[3] T. B. Calhoun, M. T. Bishop, C. H. Eichler e R. E. Lee, “Development and testing of an electro-mechanical relay to detect fallen distribution conductors,” IEEE Transactions on Power Apparatus and Systems, 1982.
[4] S.J. Balser, K.A. Clements, e D.J. Lawrence, A microprocessor-based technique for detection of high impedance faults, IEEE Trans. Power Deliv. 1 (3) (1986) vn.
[5] H.-Y.C.a.M.-T.C. Ching-Lien Huang, Algorithm comparison for high impedance fault detection based on staged fault test, IEEE Trans. Power Deliv. 3 (4) (1988) 1427–1435.
[6] A.E. Emanuel, D. Cyganski, J.A. Orr, S. Shiller, e E.M. Gulachenski, High impedance fault arcing on sandy soil in 15kV distribution feeders: contributions to the evaluation of the low frequency spectrum, IEEE Trans. Power Deliv. 5 (1990) 676–686. April.
[7] F.L. Vieira, J.M.C. Filho, P.M. Silveira, C.A.V. Guerrero, e M.P. Leite, High impedance fault detection and location in distribution networks using smart meters, 18th International Conference on Harmonics and Quality of Power (ICHQP), Ljubljana, 2018, pp. 1–6.
[8] C.V.S. Malagodi, Protection system for high impedance faults, PhD thesis, Master's thesis, University of São Paulo, 1997 (in Portuguese).
[9] F. V. Lopes, W. C. Santos, D. F. Junior, W. L. A. Neves, N. S. D. Brito e B. A. Souza, “An adaptive fault location method for smart distribution and transmission grids,” IEEE PES Conference on Innovative Smart Grid Technologies (ISGT Latin America), 2011.
[10] P.R. Silva, Alternative technique for detecting high impedance faults, PhD thesis, Master's thesis, University of Minas Gerais, 1992 (in Portuguese).
[11] I. Hafidz, P. E. Nofi, D. O. Anggriawan, A. Priyadi e M. H. Pumomo, “Neuro wavelet algortihm for detecting high impedance faults in extra high voltage transmission systems,” 2nd International Conference Sustainable and Renewable Energy Engineering (ICSREE), Hiroshima, pp. 97-100, 2017.
[12] W. C. Santos, F. V. Lopes, N. S. D. Brito, B. A. Souza, D. Fernandes Jr., W. L. A. Neves, “High impedance fault detection and location based on eletromagnetic transient analysis”, in International Conference on Power Systems Transients (IPST2013) in Vancouver, Canada, July, pp. 18-20, 2013.
[13] S. AsghariGovar, P. Pourghasem, H. Seyedi, High impedance fault protection scheme for smart grids based on WPT and ELM considering evolving and cross-country faults, Int. J. Electr. Power Energy Syst. 107 (2019) 412–421 May.
[14] K. Moloi, J. A. Jordaan and Y. Hamam, "A hybrid method for high impedance fault classification and detection," 2019 Southern African Universities Power Engineering Conference/Robotics and Mechatronics/Pattern Recognition Association of South Africa (SAUPEC/RobMech/PRASA), Bloemfontein, South Africa, 2019, pp. 548-552. doi: 10.1109/RoboMech.2019.8704765.
[15] D.P.S. Gomes, C. Ozansoy, e A. Ulhaq, High-sensitivity vegetation high-impedance fault detection based on signal's high-frequency contents, IEEE Trans. Power Deliv. 33 (3) (2018) 1398–1407 June.
[16] H.-G. Yeh, D.H. Tran, R. Yinger, High impedance fault detection using orthogonal transforms, 2014 IEEE Green Energy and Systems Conf. (IGESC), Long Beach, CA, USA, 2014, pp. 67–72 November.
[17] V. Torres, J. Guardado, H. Ruiz, e S. Maximov, Modeling and detection of high impedance faults, Int. J. Electr. Power Energy Syst. 61 (2014) 163–172 October.
[18] É.M. Lima, C.M. dos Santos Junqueira, N.S.D. Brito, B.A. de Souza, R. de Almeida Coelho, H. Gayoso Meira Suassuna de Medeiros, High impedance fault detection method based on the short-time Fourier transform, IET Gen. Transm. Distrib. 12 (11) (2018) 2577–2584, https://doi.org/10.1049/iet-gtd.2018.0093 19 6.
[19] M. Farajollahi, A. Shahsavari e H. Mohsenian-Rad, “Location identification of high impedance faults using synchronized harmonic phasors,” IEEE Power & Energy Society Innovative Smart Grid Technologies Conference (ISGT), Washington, DC, pp. 1-5, 2017.
[20] R.M. Nakagomi, ‘Proposing a system of high impedance faults in distribution networks, PhD thesis, Master's thesis, University of São Paulo, 2006 (in Portuguese).
[21] W. G. Dalzell and C. F. N. Cowan, "Blind channel shortening of ADSL channels with a single-channel linear predictor," 2011 19th European Signal Processing Conference, Barcelona, 2011, pp. 2195-2199.
[22] G. H. Riahy e M. Abedi, “Short term wind speed forecasting for wind turbine applications,” Science Direct, pp. 35-41, 2007.
[23] S. Santoso, E.J. Powers, W.M. Grady, Power quality disturbance data compression using wavelet transform methods, IEEE Trans. Power Deliv. 12 (3) (July 1997) 1250–1257.
[24] S.J. Balser, K.A. Clements, D.J. Lawrence, A microprocessor-based technique for

detection of high impedance faults, IEEE Trans. Power Deliv. 1 (3) (1986) vn.
[25] M. G. M. Zanjani; H. K. Kargar; M. G. M. Zanjani, “High impedance fault detection of distribution network by phasor measurements units”. SGRE, 2013.

Reginaldo B. G. Grimaldi was born in 1994 in Feira de Santana, Bahia, Brazil. He obtained the B.Sc. degree in Electrical Engineering in 2018 (UFS). Since 2018, he has been a masters student in the Federal University of Sergipe (UFS). His research interests include high impedance fault, power signal processing, power quality, especially on applications that involve fault detection and classification in electric systems.

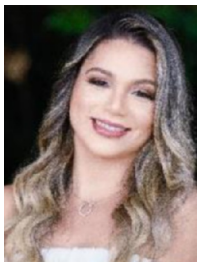

Talita S. A. Chagas was born in 1994 in Aracaju, Sergipe, Brazil. She obtained the B.Sc. degree in Electrical Engineering in 2018 from the University of Sergipe (UFS). Since 2018, she has been a masters student in the UFS, in electrical systems. Her research interests include power quality disturbances, faults in electrical power systems, power signal processing, power quality, especially on applications that involve fault identification, detection and classification in electric systems.

Jugurta Montalvão was born in Aracaju, Brazil, in 1968. He received the title of Electrical Engineer (1992) from the University of Campina Grande (UFPB II), Master in Electrical Engineering (1995) from the University of Campinas (UNICAMP) and Doctor in “Automatique et traitement du signal” (2000) from the University Paris-Sud XI. He joined the Department of Electrical Engineering of the Federal University of Sergipe (UFS) in 2005. His main research interests are pattern recognition and signal processing.

Núbia S. D. Brito was born in Antenor Navarro, Brazil, in 1965. She received the B.S. and Ph.D. degrees in electrical engineering from the Federal University of Paraíba, Campina Grande, Brazil, in 1988 and 2001, respectively, and the M.S. degree from Campinas State University, Campinas, Brazil. Currently, she is a Professor with the Department of Electrical Engineering, Federal University of Campina Grande, Campina Grande. Her research activities are mainly focused on power quality, especially on applications that involve fault detection and classification in electric systems.

Wellinsílvio C. dos Santos Wellinsílvio C. Santos (STM'11-M'16) He received his B.Sc., M.Sc., and D. Sc. degrees in Electrical Engineering from Federal University of Campina Grande (UFCG), Brazil, in 2009, 2011, and 2016 respectively. He works currently as a professor at the Technology Center at Federal University of Alagoas (UFAL). His research activities are mainly focused on electromagnetic transients, high impedance fault modeling, and power quality.

Tarso V. Ferreira was born in 1980 in Aracaju, Sergipe, Brazil. He received the B.Sc., M.Sc., and D.Sc. degrees in electrical engineering from Federal University of Campina Grande (UFCG), Paraíba, Brazil, in 2005, 2007, and 2011, respectively. From 2008 to 2017 he worked as a professor at UFCG, and since then works in the same position at the Federal University of Sergipe. He is also member of Graduate Program in Electrical Engineering at UFCG and Research Fellow at INESC P&D Brazil. His research interests include high-voltage equipment, electric field mapping, digital signal processing and insulation systems.